Asymmetric Flow Field-Flow Fractionation (AF4) with Fluorescence Detection for Direct, Real-Time, Size-Resolved Measurements of Drug Release from Polymeric Nanoparticles

Sheyda Shakiba[a], Carlos E Astete[b], Rafael Cueto[c], Debora F Rodrigues[a], Cristina M Sabliov[b], Stacey M Louie[a]*

[a] Department of Civil & Environmental Engineering, University of Houston, Houston, TX 77004, United States

[b] Department of Biological & Agricultural Engineering, Louisiana State University, Baton Rouge, LA 70803, United States

[c] Department of Chemistry, Louisiana State University, Baton Rouge, LA 70803, United States

*Corresponding author

Phone: 713-743-8646; Fax: 713-743-4260; Email: slouie@uh.edu

Abstract

Polymeric nanoparticles (NPs) are typically designed to enhance the efficiency of drug delivery by controlling the drug release rate. Hence, it is critical to obtain an accurate drug release profile. This study presents the first application of asymmetric flow field–flow fractionation (AF4) with fluorescence detection (FLD) to characterize release profiles of fluorescent drugs from polymeric NPs, specifically poly lactic-*co*-glycolic acid NPs loaded with enrofloxacin (PLGA-Enro NPs). In contrast to traditional release measurements requiring separation of entrapped and dissolved drugs (typically by dialysis) prior to quantification, AF4-FLD provides *in situ* purification of the NPs from unincorporated drugs, along with direct measurement of the entrapped drug. Size distributions and shape factors are simultaneously obtained by online dynamic and multi-angle light scattering detectors. The AF4-FLD and dialysis approaches were compared to evaluate drug release from PLGA-Enro NPs containing a high proportion (≈ 88%) of unincorporated (burst release) drug at three different temperatures spanning the glass transition temperature (30 °C for PLGA-Enro NPs). The AF4-FLD analysis was able to identify size-dependent release rates across the entire continuous NP size distribution, with smaller NPs showing faster release. The AF4-FLD method also clearly captured the expected temperature dependence of the drug release (from almost no release at 20 °C to rapid release at 37 °C). In contrast, dialysis was not able to distinguish these differences in the extent or rate of release of the entrapped drug because of interferences from the burst release background, as well as the dialysis lag time. A mechanistic diffusion model that integrates data from both AF4-FLD and dialysis further supported the advantages of AF4-FLD to capture the true release rate of entrapped drug and avoid artifacts observed in dialysis. Overall, this study demonstrates the novel application and unique advantages of AF4-FLD methods to obtain direct, size-resolved release profiles of fluorescent drugs from polymeric NPs.

Keywords:

Polymeric nanoparticles; Release profile; Method development; Asymmetric flow field–flow fractionation; Fluorescent drug; Dialysis

1. Introduction

Drug entrapment in polymeric nanoparticles (NPs) is a well-known approach to enhance drug efficiency by controlling the drug transport, uptake, and release [1-4]. Potential benefits conferred by drug entrapment include reduction in drug administration frequencies, decreased toxicity to cells, and targeted delivery [5-9]. Accurate characterization of the drug distribution (entrapped versus dissolved) and release profile is crucial to understand or predict the performance of drug-loaded NPs, with release profile being one of the key quality attributes specified in U.S. Food & Drug Administration (FDA) guidelines for evaluation of nanomaterial-based drugs [10]. Characterizing the release behavior across different environmental conditions such as pH, temperature, or media composition can also provide insight into the mechanisms of release [11, 12]. For example, heating the polymeric nanoparticle beyond its glass transition temperature (T_g) is expected to result in higher diffusion and release rates of drugs from the polymeric matrix [11, 13, 14]. Methods to obtain release profiles should hence be robust to accurately evaluate drug release across a variety of release conditions.

Direct measurements of the drug entrapped within the NPs (Figure 1a) can be advantageous to monitor drug loading and release over traditional dialysis experiments (Figure 1b), in which the dissolved drugs are quantified in the dialysate, e.g., by high performance liquid chromatography (HPLC), or the total drug in the retentate (dissolved and entrapped) is measured by extracting or dissolving the NPs in an organic solvent for drug quantification. Dialysis introduces an unavoidable lag time for dissolved drugs to diffuse through the dialysis membrane; if this lag time is the limiting rate (i.e., slower than the NP release rate), then the release rate from the NPs can be underestimated. For example, using a drug-selective electrode to eliminate the dialysis lag time found a faster release from microgels than dialysis [15]. Furthermore, a high “burst” release of

unincorporated or loosely-bound drugs can obscure the subsequent release of lower concentrations of the entrapped drugs, resulting in erroneous interpretation of both the extent and rate of release from within the NPs. Methods to directly probe specifically the entrapped drug in the NPs in "real time" (i.e., without any separation lag) would hence be advantageous to eliminate these artifacts.

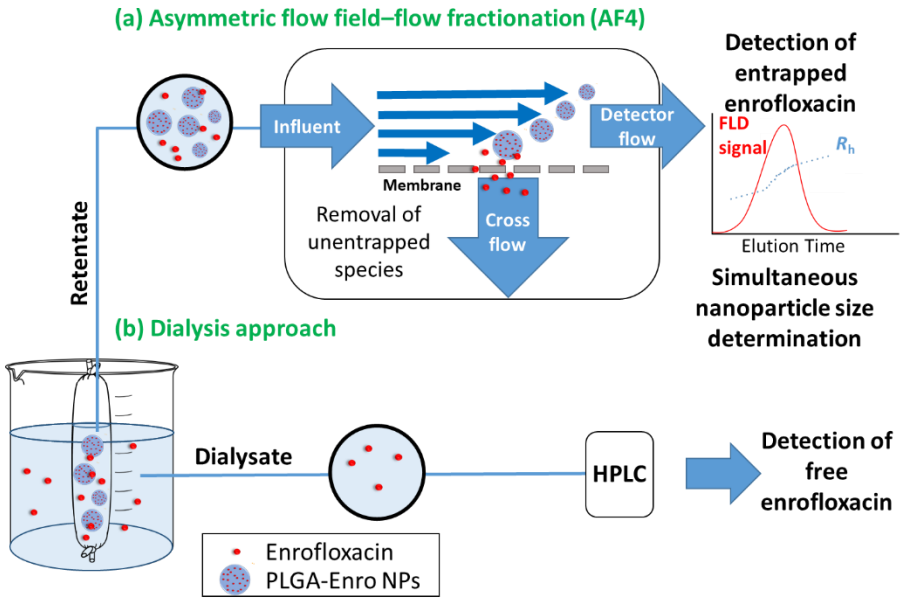

Figure 1. Schematic comparing asymmetric flow field–flow fractionation (AF4) (a), and dialysis (b). AF4 provides direct measurement of entrapped drugs together with *in situ* purification to remove unentrapped drugs and simultaneous nanoparticle size distribution analysis. This figure is adapted from the previously published work by Shakiba et al. [4].

Asymmetric flow field–flow fractionation (AF4) is proposed here to provide real-time separation of entrapped and dissolved drugs and enable direct analysis of the NP-entrapped drugs (Figure 1a). The principle of AF4 is discussed in previous texts [16-22]; briefly, injected particles are first "focused" toward an accumulation wall (an ultrafiltration membrane). Then, an applied crossflow establishes a force field, in which smaller particles (with higher diffusion coefficient) equilibrate toward the middle of channel (with maximum velocity) and elute from the AF4 channel

sooner than larger particles. AF4 hence provides immediate removal of dissolved species that wash through the membrane during focusing, in addition to NP size separation. NP sizes, compositions, and concentrations can then be characterized by coupling AF4 to various spectroscopic and light scattering detectors [23]. In the vast majority of applications thus far, AF4 has primarily been coupled with light scattering to obtain size distributions of polymeric NPs [24-30] or with inductively coupled plasma mass spectrometry (ICP-MS) for inorganic NP speciation [31-35]. Few studies have applied AF4 to assess the loading of organic drug molecules in polymer NPs. Recently, Hu et al. evaluated the drug distribution across different NP size fractions by collecting AF4 fractions followed by offline HPLC analysis [36]. Hinna et al. and Fraunhofer et al. investigated the feasibility of coupling AF4 with online UV-Vis analysis to directly probe loading or transfer between liposomal and gelatin NPs, respectively [37-40]. However, a major limitation of UV-Vis detection is the interference from particle scattering [37, 41], which restricts measurements to only NPs with high analyte entrapment and can make quantification infeasible for larger NPs (with high scattering intensities) with low drug loading [37].

Fluorescence detection (FLD) can be a more sensitive and selective alternative to UV-Vis detection for fluorescent or fluorescently-labeled compounds [42-44]. While AF4 has been coupled with FLD to characterize macromolecules [45] such as humic substances [46-49], proteins [42, 43, 50], and biopolymers [51], it has not yet been used to quantify drug loading inside the polymeric NPs. Iavicoli et al. evaluated the binding of fluorophore-tagged peptides to liposomes by coupling AF4 with either UV-Vis or FLD, but FLD was only used for qualitative confirmation of binding since UV-Vis detection was reported to provide more reproducible and linear quantification of the peptide [52]. However, FLD was also reported to be more sensitive than UV-Vis detection. Hence, the high sensitivity and selectivity of FLD are expected to be advantageous

for NPs with low drug loading that are not amenable to UV-Vis quantification. Furthermore, combining AF4 for NP size separation with FLD for drug quantification would hypothetically enable unique measurements of size-resolved drug release profiles to be achieved.

The objective of this study is to demonstrate the novel development of an AF4-FLD method for the acquisition of direct, real-time, size-resolved release profiles of fluorescent drugs from polymeric NPs and to evaluate the advantages of AF4-FLD over existing dialysis and AF4-UV methods. Here, enrofloxacin-loaded poly lactic-*co*-glycolic acid (PLGA) NPs are evaluated as a model system [9], where PLGA is one of the most common polymers for drug delivery systems [5, 6, 53], and enrofloxacin is a fluoroquinolone antibiotic with inherent fluorescence. First, method development is demonstrated on coupling AF4 with FLD and UV detection to evaluate enrofloxacin entrapment in PLGA NPs, along with online multi-angle light scattering (MALS) and dynamic light scattering (DLS) detectors to acquire NP size distributions and shape factors. Then, the AF4-FLD method is applied to evaluate the size- and temperature-dependent drug release from the NPs, and the AF4 results are contrasted to traditional dialysis experiments. A diffusion model is applied that explicitly considers both diffusion barriers (through the polymeric matrix, and across the dialysis membrane) to integrate the AF4 and dialysis data and quantify release rates. This study ultimately demonstrates the first proof of concept of AF4-FLD to monitor drug release from polymeric NPs and the significant and unique advantages achieved over alternative methods.

2. Experimental Section

2.1. Materials

Potassium phosphate monobasic anhydrous, sodium phosphate dibasic heptahydrate (both ACS grade, Amresco, Solon, OH), sodium chloride (> 99.0%, ACS grade), and potassium chloride

99.999% (trace metal basis) (Acros Organics, NJ) were used to prepare phosphate buffered saline (PBS, 137 mM NaCl, 2.7 mM KCl, 10.1 mM Na_2HPO_4, 1.8 mM KH_2PO_4, pH 7.4). Phosphoric acid (85%, ACS grade, Ricca Chemical Company, Arlington, TX) and acetonitrile (Chromasolv Plus, for HPLC, >99.9%, Honeywell Riedel-de Haen, Seelze, Germany) were used for HPLC mobile phase preparation. Enrofloxacin (Alfa Aesar, Ward Hill, MA) was purchased to prepare calibration standards. Poly lactic-*co*-glycolic acid (PLGA), poly (vinyl alcohol) (PVA), Tween 80, and enrofloxacin from Sigma Aldrich (Millipore Sigma, St Louis, MO), ethyl acetate (ACS grade, ≥99.5%, Fisher Scientific Co, Pittsburgh, PA), and trehalose dihydrate (≥98%, Fisher Scientific Co) were used in the NP synthesis.

2.2. NP synthesis

The NPs were synthesized by emulsion evaporation similarly to our prior work except substituting the PVA surfactant with Tween/PVA [9, 54]. Briefly, for the enrofloxacin-loaded PLGA NPs (denoted hereafter as "PLGA-Enro NPs") the organic phase was prepared by dissolving 400 mg of PLGA and 40 mg of enrofloxacin in 10 mL of ethyl acetate under mild stirring for 30 minutes. The aqueous phase was prepared by dissolving Tween 80 in 90 mL of low resistivity water to obtain a final concentration of 5 mg/mL. Next, the organic phase was poured into the aqueous phase under strong stirring, and the emulsion was passed four times in a microfluidizer (M 110P, Microfluidics, Westwood, MA). Next, the organic solvent was evaporated in a rotavapor (Buchi R-300, Buchi Corp., New Castle, DE) under vacuum at 32 °C for 70 minutes. Then, the polymeric NP suspension was mixed with 5.6 mL of 2.0% (w/v) of PVA solution prepared in advance with water of low resistivity. Finally, the suspension was mixed with 1.1 g of trehalose and freeze dried (FreeZone 2.5, Labconco Corp., Kansas City, MO) at -80 °C for 2 days.

The samples were stored at -20 °C for testing and characterization purposes. “Empty” PLGA NPs were synthesized following the same method with the exclusion of enrofloxacin. The mixtures did not undergo purification or separation steps prior to lyophilization, and hence the total concentration of enrofloxacin in the lyophilized PLGA-Enro powder was 2.0 wt. %.

2.3. NP entrapment efficiency

To obtain the entrapment efficiency of the PLGA-Enro NPs, the lyophilized powder was dispersed in PBS at a concentration of 0.5 g/L, and the dissolved drug was immediately separated from the NPs using two different approaches and quantified by UV absorbance at 270 nm on a UV−2600 spectrophotometer (Shimadzu, Columbia, MD). In the first approach, 4 mL of the PLGA-Enro NPs (0.5 g/L in PBS) were filtered in pre-washed 100 kDa Amicon Ultra-4 centrifugal filters (EMD Millipore, Burlington, MA) at 4500 rpm (relative centrifugal force (RCF), RCF_{min} = 1879 g and RCF_{max} = 4415 g) for 8 min (Sorvall Legend XTR Centrifuge, Thermo Fisher Scientific, Waltham, MA), and the filtrate was collected for analysis. In the second approach, the supernatant of 20 mL of PLGA-Enro NPs (0.5 g/L in PBS) was collected after ultracentrifugation for 30 min at 40 000 rpm (Optima L-80 XP ultracentrifuge, Beckman Coulter Inc., Indianapolis, IN). The entrapped drug concentration in the NPs was obtained by subtracting the supernatant (or filtrate) concentration from the total concentration of enrofloxacin added during the synthesis.

2.4. Differential scanning calorimetry

The glass transition temperature (T_g) of the PLGA-Enro NPs was measured by differential scanning calorimetry (DSC). The measurements were obtained on a TA Instruments DSC (model Q200, TA Instruments, New Castle, DE). The DSC experiments were performed with 5 to 10 mg

of sample using standard aluminum pans. The sample compartment was purged with nitrogen (gas flow 50 mL/min) during the experiment. The procedure was as follows: (1) cool down sample to -40 °C; hold isothermal at this temperature for 5 min; (2) first heating scan to 80 °C at 10 °C/min; (3) equilibrate again at - 40 °C; hold isothermal at this temperature for 5 min; (4) second heating scan from -40 °C to 80 °C at 10 °C/min. The T_g and onset and offset points were calculated from the second heating curve using the inflection point method.

2.5. Release experiments

Release experiments were conducted using a stock suspension of PLGA-Enro NPs, prepared at 15 g/L in PBS (pH 7.4) with bath sonication for 10 seconds (Branson 1800, Emerson, St. Louis, MO). 1 mL of the NP suspension was added to a 1 mL dialysis device (Spectra/Por Float-A-Lyzer G2, molecular weight cut-off (MWCO) 100 kDa, cellulose ester), which was prewashed following the manual. The MWCO was chosen to be much higher than enrofloxacin to improve drug diffusion from the dialysis device into the reservoir [15, 55]. Release experiments were conducted at three different temperatures: room temperature (20 ± 1) °C, (28 ± 1) °C, and (37 ± 1) °C, where room temperature was measured by both a digital thermometer in the lab and a thermometer held inside the water bath, and the higher temperatures were achieved in a heated bath sonicator (Branson 1800, Emerson, St. Louis, MO) without sonication. The dialysis device was floated in a closed (screw-cap) reservoir containing 120 mL fresh PBS preheated and equilibrated for 24 h in advance. At each time point, for AF4 measurements, 20 μL of NPs from inside the dialysis device was diluted with 280 μL PBS to obtain a final concentration of 1 g/L of NPs, then immediately injected to the AF4 instrument (method presented below). Simultaneously, for HPLC measurements, 1 mL of liquid from the reservoir was collected and substituted with 1

mL fresh PBS and held refrigerated for further quantification by HPLC (method below). Because samples were removed from inside and outside the dialysis device for analysis, the mass of NPs and drug in the system is depleted between each measurement. As such, the released concentration obtained by HPLC was corrected to account for sample removal (details in the Supporting Information (SI)). All experiments were duplicated on independently prepared NP suspensions.

Control experiments were also performed for enrofloxacin (300 mg/L in PBS) without NPs at the three temperatures above to obtain the diffusion rates of drug from the dialysis device. At each time point, 10 μL was collected from inside the dialysis device and diluted with 380 μL PBS, and 400 μL was collected from the reservoir (and substituted with the equivalent volume of fresh PBS) for HPLC analysis. A mass balance on the measured retentate and dialysate concentrations at different time points indicated no significant loss of enrofloxacin to the membrane. All experiments were duplicated.

2.6. AF4 method for direct analysis of NPs

The AF4 module (Eclipse AF4, Wyatt Technology, Santa Barbara, CA) was integrated with an Agilent 1290 Infinity HPLC system (Agilent, Santa Clara, CA) comprising a binary pump, degasser, and autosampler. The Eclipse AF4 short channel was prepared with a spacer height of 250 μm and 10 kDa regenerative cellulose (RC) membrane. The mobile phase was the same PBS as the dialysis media. The injection and detector flow rates were 0.2 mL/min and 0.5 mL/min, respectively. The injection volume was 50 μL and total run duration was 100 minutes for each sample. The complete AF4 schedule is presented in the SI Table S1, including the duration and flow rates used during focusing and elution.

Online detectors included an Agilent 1260 Infinity UV-Vis diode array detector (DAD)

and fluorescence detector (FLD), as well as a Wyatt DAWN HELEOS II multi-angle light scattering (MALS) detector and online Wyatt dynamic light scattering (DLS) (or quasi-elastic light scattering) detector. The DLS detector was placed at 140° scattering angle, and measurement duration was 5 s. The UV DAD was set to monitor the 400 nm wavelength and collect full spectra from wavelength 190 nm to 600 nm (step 2 nm). For FLD, the optimal excitation and emission wavelengths were set as 280 nm and 420 nm, respectively, with a photomultiplier tube (PMT) gain of 13. Emission spectra were also collected at each time point at a fixed excitation wavelength (280 nm) with emission wavelength varying from 300 nm to 540 nm (5 nm step size). The optimization of the flow parameters and detector setup, as well as the analysis to monitor enrofloxacin release from the NPs, are discussed in detail in the Results and the SI.

2.7. HPLC method for analysis of dissolved enrofloxacin

Dissolved enrofloxacin was quantified by HPLC on the Agilent 1290 Infinity HPLC system noted above, using a ZORBAX Eclipse Plus C18 HPLC column (4.6 × 150 mm dimensions, 5 µm particle size). Isocratic elution was performed with phosphate buffer (0.02 M, pH 3) (82%) and acetonitrile (18%) as the mobile phase [56], flow rate of 1 mL/min, and run duration of 10 minutes. The injection volume was 10 µL. The UV DAD was set to monitor the 280 nm wavelength and collect full spectra from 190 nm to 600 nm (step size 2 nm). The optimum FLD setting for enrofloxacin (excitation and emission wavelengths of 280 nm and 450 nm, respectively) was identified on repeated injections by first fixing the excitation wavelength and determining the maximum emission wavelength, then identifying the maximum excitation wavelength at the optimized emission wavelength. FLD spectra were also collected with excitation fixed at 280 nm and emission wavelength from 300 nm to 540 nm (step size 5 nm) and PMT gain set at 8. The

difference in optimal FLD emission wavelengths for PLGA-Enro NP analysis by AF4 and dissolved enrofloxacin analysis by HPLC is discussed in the Results.

2.8. Batch measurements of NP size and zeta potential

NPs were dialyzed at 20 °C and 37 °C following the same procedure as the release experiments, with NP samples collected and diluted into PBS as for AF4. Batch DLS and electrophoretic light scattering measurements of size and zeta potential, respectively, were taken on a Malvern Zetasizer Nano ZS instrument (Malvern Panalytical Inc., Malvern, UK). Zeta potential measurements were conducted in folded zeta capillary cells (DTS 1070, Malvern) and computed from the electrophoretic mobility using the Smoluchowski model and the average and standard deviations across five measurements were reported.

3. Results and Discussion

3.1. Method development for separation and evaluation of PLGA-Enro NPs by AF4-FLD

First, we demonstrate the development of AF4 with four detectors (UV, FLD, MALS, and DLS) to evaluate the drug loading and release profile along with the size distribution of NPs. Separately from the AF4 analysis, the initial concentration of entrapped enrofloxacin was determined to be (3.2 ± 0.5) μg/mg (n = 3 replicates) or (1.5 ± 0.1) μg/mg (n = 2 replicates) after immediately dispersing and separating the PLGA-Enro NPs using ultrafiltration or ultracentrifugation, respectively. Ultrafiltration may overestimate the entrapment due to losses of dissolved enrofloxacin to the filter membrane, whereas ultracentrifugation may underestimate entrapment if the strong centrifugal forces induce compression of the NPs and release of enrofloxacin. Averaging the two methods, the entrapment was ≈ (2.3 ± 1.1) μg/mg, and the

entrapment efficiency relative to the total enrofloxacin (2.0 wt. %) in the PLGA-Enro NPs was ≈ 12%. Note that because the NPs were not purified prior to subsequent use, a high burst release (≈ 88%) of unincorporated or rapidly desorbed drug also occurs in all following experiments, but this burst release is removed *in situ* during the AF4 measurement.

AF4 method development includes optimization of the AF4 flow parameters and the detector settings used for characterization. For simplicity, we first present the results of the optimized AF4 method, then discuss the detector and flow optimization. Figure 2 shows the optimized AF4 chromatograms with UV, FLD, and LS detection for both PLGA-Enro and empty PLGA NPs, as well as the hydrodynamic radius (R_h) obtained by online DLS. Satisfactory size separation of the NPs was achieved, with elution of smaller NPs followed by larger NPs. Furthermore, a strong fluorescence signal for the entrapped enrofloxacin is observed in the PLGA-Enro NPs but not in the empty PLGA NPs.

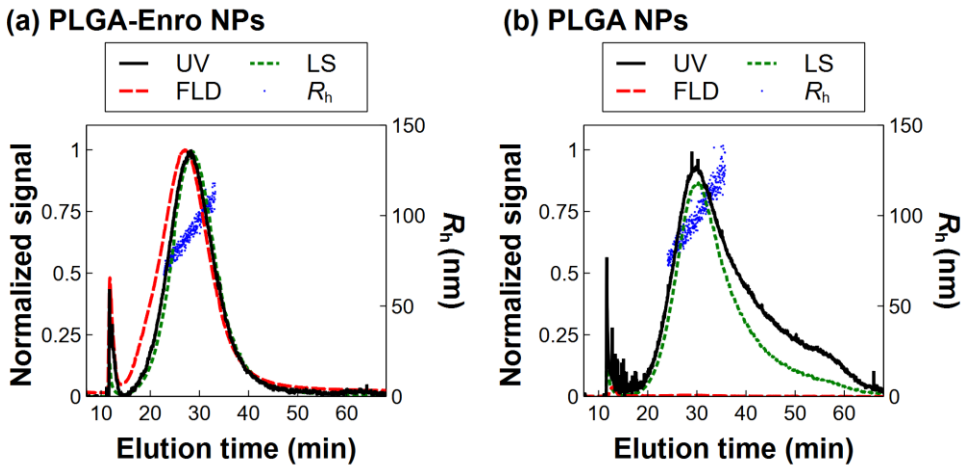

Figure 2. AF4 chromatograms with UV_{400}, FLD, and LS detection and simultaneous R_h analysis by online DLS for PLGA-Enro NPs (a) and "empty" PLGA NPs (b). NPs were injected at 1 g/L in PBS using the AF4 flow and injection schedule in SI Table S1. The excitation and emission

wavelengths for FLD detector were set at 280 nm and 420 nm, respectively, and the LS signal shown is at 90° scattering angle. All signals were normalized to their maximum value in the corresponding PLGA-Enro chromatogram (a). R_h is plotted across the full width at half maximum (FWHM) of the DLS count rate peak.

The potential to quantify entrapped enrofloxacin by either UV-Vis or FLD was thoroughly investigated by comparing the spectra of the NPs eluting in AF4 (with *in situ* drug removal) to the unpurified NPs (injected to the AF4 channel in elution mode only without focusing or crossflow, and hence without removal of the dissolved drug). Both detectors show that the high burst release of enrofloxacin is indeed eliminated in AF4, while the NPs and entrapped drug are retained in the channel for analysis. Although prior AF4 methods have utilized UV-Vis detection for entrapped drug quantification [37-40, 52], here UV-Vis was not suitable to quantify enrofloxacin in the PLGA-Enro NPs because the UV absorbance attributable to the drug was low relative to the particle scattering (SI, Figure S1a and Figure S3), such that scattering corrections used in prior AF4-UV studies [37] were not feasible. Rather, the FLD produced a significantly more sensitive and selective detection of the enrofloxacin in the PLGA matrix (SI, Figure S1b). Quantification of the enrofloxacin inside the NPs against external calibration standards of dissolved enrofloxacin (injected into the AF4 without crossflow) by FLD was attempted but yielded a higher NP entrapment of (5.2 ± 0.5) μg/mg (n = 15 replicates) than that obtained above by measuring the dissolved drug, suggesting strong fluorescence enhancement in the PLGA matrix. In addition, a shift in the peak fluorescence emission wavelength can be observed when comparing the entrapped enrofloxacin to the dissolved enrofloxacin, also suggesting a strong interaction between the enrofloxacin and PLGA matrix (SI, Figure S1b). Because calibration against external standards

was not possible, we note that a separate measurement of entrapment efficiency is first required to determine the initial drug loading, and the FLD can subsequently be used to evaluate the relative proportion of drug remaining in the NPs as described hereafter.

Another challenge in AF4 for quantitative analysis of NPs is the possibility for inconsistent NP concentrations across measurements, either because of changes to the sample (e.g., solvent evaporation or losses of NPs) or variability in recovery of NPs from the AF4 channel during the measurement. To overcome this problem, we normalize the FLD peak area corresponding to the entrapped enrofloxacin to the UV peak area at 400 nm. Enrofloxacin has negligible absorbance at 400 nm (SI, Figure S1a); therefore, the UV signal at 400 nm mainly corresponds to the PLGA NPs, as supported by the similar UV signals in the PLGA-Enro and empty PLGA NPs (Figure 2). Note that while the use of FLD to evaluate peptide binding to liposomes was previously reported to show poorer reproducibility and linearity than UV detection [52], here we achieve a relative standard deviation of 11% on the raw FLD peak areas and 9.4% on the ratio of FLD/UV peak areas (n = 15 replicates), whereas the UV detector was unsuitable for entrapped enrofloxacin quantification. To obtain release profiles over time, we assume the FLD/UV ratio to be linearly proportional to the entrapped drug concentration and evaluate the percent release relative to the FLD/UV ratio measured at time zero (immediately upon dispersing the NPs in solvent).

Optimization of the duration and flow rates of each step in the AF4 method typically revolves around achieving good size separation (by adjusting the focus flow rate or duration to focus the NPs into a narrow band against the accumulation wall and adjusting the crossflow rate in the elution step to achieve good resolution of different NP sizes) and good overall recovery with minimal perturbation of the NPs (for example, deformation of fragile NPs) [16]. However, for entrapped drug quantification, the potential for drug washout from the NPs during the focus step

must also be considered [18, 57, 58]. Here, three focus flow rates (0.5 mL/min, 1.5 mL/min, and 2.0 mL/min) and two focus durations (4 min and 8 min) were compared (SI, Figure S2). Longer focus durations and, to a lesser extent, higher focus flow rates resulted in lower drug recoveries by FLD. The lowest focus flow rate tested resulted in a large initial "void" peak eluting immediately after the focus step and prior to the main NP peak, which may represent incomplete NP relaxation in the channel or excess (unincorporated) polymeric material with adsorbed enrofloxacin that is not fully removed with shorter focusing times (SI, Table S2). Hence, a moderate focus flowrate (1.5 mL/min) and shorter focus duration (4 min) were selected as the optimal conditions.

The mass recovery of NPs, evaluated by comparing the UV area (at 400 nm) of the NPs in AF4 to that obtained without focusing or crossflow, was not significantly affected by the focus flow rate or duration. In the optimized conditions (Figure 2), NP recovery was (64 ± 7) % (n = 12 replicates) and (66 ± 7) % (n = 12) in the main NP peak or the main and void peaks together, respectively. A rinse peak can also be observed during a final rinse through the injection port at the end of each measurement (SI, Figure S2) and likely represents adsorption of NPs in the AF4 injection port. Inclusion of this peak increases NP recovery to (81 ± 13) % (n = 12), but the low FLD/UV signal suggests a lack of drug (e.g., due to washout). Therefore, to obtain the drug release profiles, the washout peak is excluded from the analysis. Additionally, although the void peak also contains enrofloxacin (SI, Figure S4), it is also excluded from the analysis since the identity (excess polymer or NPs) is not clear; however, including this peak does not significantly change the conclusions of the analyses (SI, Figure S5). We note that some entrapped drugs may still be washed out from the NPs in the optimized AF4 method, but we assume the fraction of washout is consistent across all measurements (with consistent AF4 settings) and hence that the semi-quantitative analysis of entrapped drug relative to the time zero measurement is valid.

3.2. AF4 measurements show size- and temperature-dependent release profiles

The optimized AF4 method was applied to acquire direct release profiles on the PLGA-Enro NPs and compared to a traditional, indirect approach (dialysis with quantification of drug release to the dialysate). Temperature is well known to influence drug release rates from polymeric NPs; notably, an increase in temperature above T_g results in the transition from a glassy to rubbery state, and faster release is expected with the increased relaxation of the polymer chains [14]. The measured T_g of the PLGA-Enro NPs was 30.3 °C (onset point 27.3 °C, offset point 33.7 °C). (SI, Figure S6). Hence, temperatures below (20 °C), near (28 °C), and above (37 °C) the T_g were applied to evaluate the capability of the AF4 and dialysis approaches to capture the expected temperature-dependent release behavior.

Figure 3 presents the AF4-UV and AF4-FLD chromatograms, and Figure 4a shows the release profile obtained by processing the AF4 data as described above, i.e., by normalizing the FLD/UV ratio at each time point to FLD/UV at time zero to obtain the relative fraction of entrapped enrofloxacin remaining in the NPs over time. The AF4 method clearly shows a strong temperature dependence of enrofloxacin release from the PLGA NPs, with minimal enrofloxacin release at 20 °C, slow release at 28 °C, and rapid release at 37 °C (above T_g). It is noted that the UV peak area (at 400 nm) increased over time (Figure 3a), more significantly at higher temperatures, perhaps due to solvent evaporation from the 1 mL dialysis device leading to concentration of the NPs over time. Hence, the FLD/UV normalization is important to correct for NP concentration and appropriately compare enrofloxacin loading in the NPs across multiple samples. However, we note the same trends are clearly observed for the raw FLD peak over time (Figure 3b) as in the FLD/UV peak area (Figure 4a), supporting the reliability of the analysis (i.e., the decreasing FLD/UV ratio is not an artifact of changing UV peak areas).

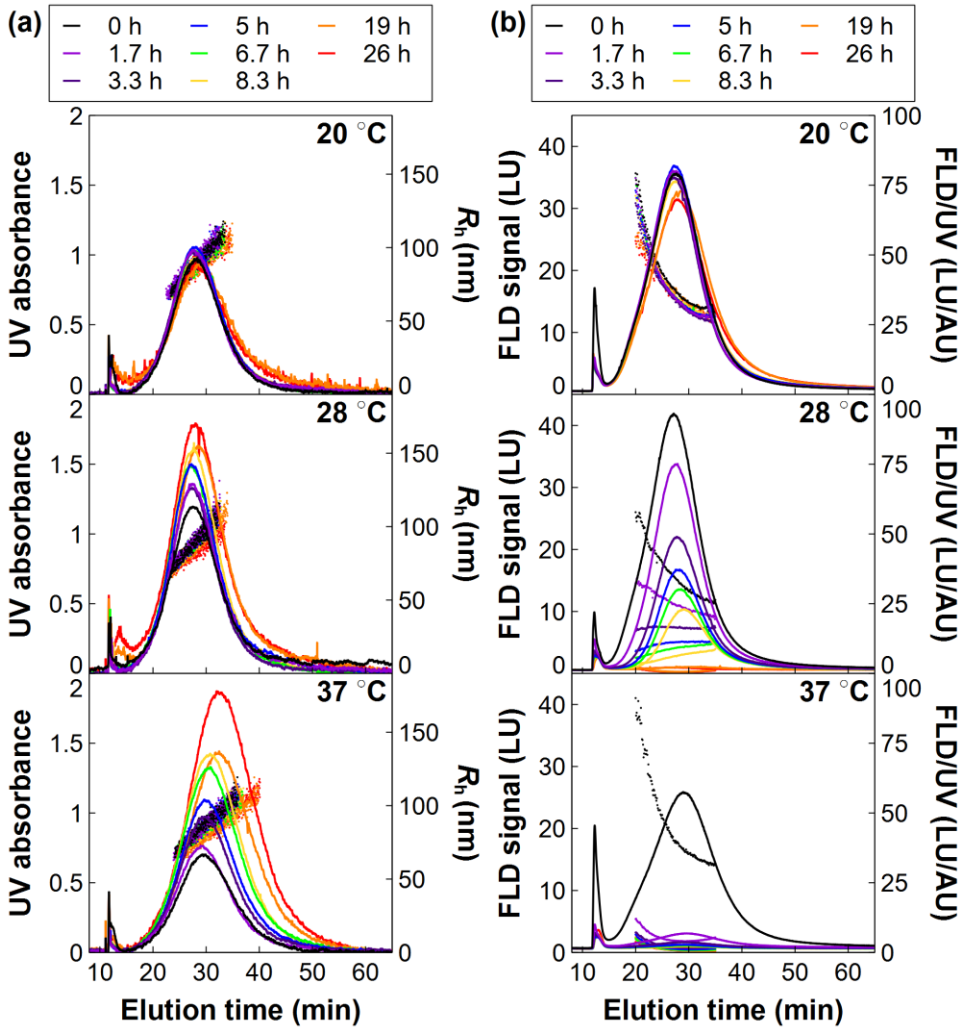

Figure 3. AF4-UV (a, solid traces, left axis) and AF4-FLD (b, solid traces, left axis) chromatograms, R_h (a, scatter points, right axis), and FLD/UV ratios (b, scatter points, right axis) of PLGA-Enro NPs were obtained from 0 to 26 h at 20 °C, 28 °C, and 37 °C. NPs were collected during dialysis and diluted to 1 g/L in PBS for AF4 analysis (AF4 settings noted in SI Table S1 and Figure 2). R_h is plotted across the FWHM of the DLS count rate peak. The FLD/UV ratio was obtained by diving the FLD signal over UV signal at each chromatographic time point. The UV and FLD chromatograms and corresponding R_h and FLD/UV are color matched. (For color matching the legends to data, color should be use for printing this figure or refer to online version of this article.)

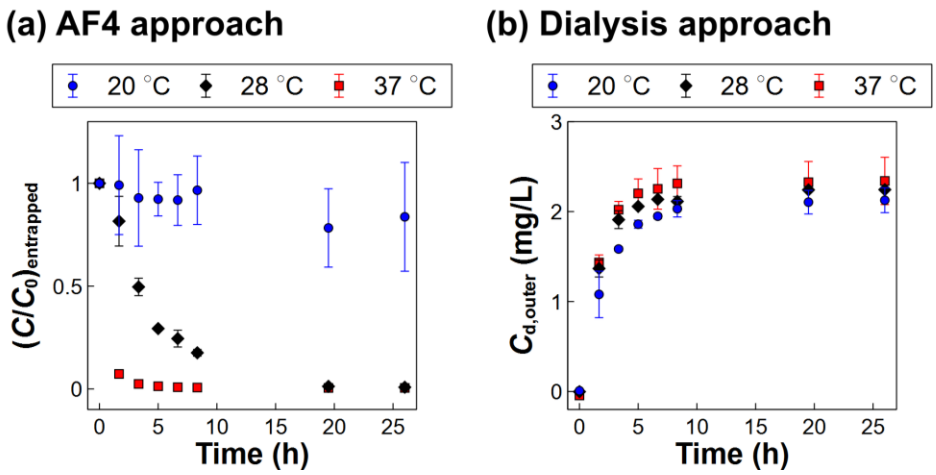

Figure 4. Release profiles of PLGA-Enro NPs by AF4-FLD (a) and dialysis (b). The AF4 release profile was obtained by normalizing the ratio of FLD/UV peak areas at each time point to that measured at time zero (AF4 settings noted in SI Table S1 and Figure 2). Error bars represent the standard deviation across two replicates.

Coupling AF4 with online DLS and MALS detectors produces additional useful information regarding the size and shape of the NPs. An increase in peak retention time (RT) and broadened peak shape was observed in the FLD and UV chromatograms (Figure 3) for the two last time points (19 h and 26 h), especially for higher temperatures (28 °C and 37 °C). First, we hypothesized this behavior may indicate a change in the NP size and polydispersity. However, the online DLS results showed no significant change in the R_h of the NPs (Figure 3a), consistent with batch DLS measurements (SI, Figure S7a). Additionally, using the MALS detector to obtain the radius of gyration (R_g), the shape factor R_g/R_h was determined to be 0.77 ± 0.01 at time zero (n=6 replicates) and also did not vary significantly over time (SI, Figure S7b), suggesting a homogenous sphere shape for the NPs [59]. This observation highlights that changes in RT and peak broadness in AF4 may not necessarily correspond to changes in NP size or morphology (e.g., swelling or agglomeration); hence, online light scattering analysis is essential.

Prior AF4 studies on polymeric NPs attributed similar increases in RT to a change in the surface charge of the NPs and therefore their interaction with the membrane [60]; however, in this study, we did not observe any significant changes in the zeta potential measurements over 26 h (SI, Figure S8). Moreover, the change in RT cannot be explained by the decreasing enrofloxacin loading in the NPs, since most of the drugs were released prior to the appearance of the RT change in the chromatograms at 37 °C. A possible explanation is loss of Tween/PVA surfactant from the NP surface over time, which could reduce repulsive interactions with the AF4 membrane. Overall, the direct size analysis by online DLS and MALS shows that the PLGA-Enro NPs were physically stable during the drug release, and hence changes in swelling or degradation of the polymeric NPs are not involved in the higher release with temperature.

Finally, the collection of both FLD and UV data across the entire continuous size distribution of NPs eluting from the AF4 channel enabled size-resolved drug release profiles to be evaluated with remarkable resolution by evaluating the FLD/UV ratio at each chromatographic time point (Figure 3b). Release rate constants were fitted at each elution time (representing different size NPs), as shown in SI Figure S9 for the release at 28 °C. A more rapid decrease in the FLD/UV ratio is clearly observed for smaller NPs (eluting earlier) than for larger NPs, as expected given the shorter diffusion distance in the smaller NPs. These results demonstrate that AF4-FLD can be a powerful tool to distinguish drug release in complex samples comprised of polydisperse NPs or several different NP populations that can be individually analyzed within a single AF4 run.

3.3. Traditional dialysis measurements are poorly sensitive to the release of entrapped drugs in the presence of a high burst release or rapid release

The AF4-FLD approach was compared to dialysis as a traditional method to acquire release

profiles, in which the concentration of drugs in the dialysate at each time point was measured by HPLC-FLD (Figure 4b). The overall release profiles obtained by dialysis appear to contradict the AF4 measurements. For example, AF4 showed a rapid release of enrofloxacin at 37 °C within < 4 h (Figures 3 and Figure 4a), whereas dialysis suggests a slower release over 10 h, similar to that at 28 °C (Figure 4b). At 20 °C, AF4 showed no significant release of entrapped drugs (Figures 3 and Figure 4a), whereas dialysis results appear to indicate a similar extent of release to the higher temperatures (Figure 4b). Overall, the dialysis results would suggest minimal differences in either the rates or extent of release, regardless of temperature. In contrast, AF4 clearly distinguishes the expected temperature dependence in the drug release rates, as well as the extent of released drug.

These seemingly inconsistent results can be attributed to the difference in the principle of each method and the presence of a high proportion of burst release of unincorporated or loosely bound drugs (≈ 88% of the total enrofloxacin) in the PLGA-Enro NPs, which can obscure quantification of the entrapped drug. The dialysate includes the total dissolved enrofloxacin (from both the burst release and subsequent release of entrapped drugs). Hence, distinguishing the release of specifically the entrapped drugs by dialysis is challenging if a high burst release occurs. Furthermore, the dialysis membrane introduces a lag time to equilibrate the dissolved drug inside and outside the dialysis device. Hence, obtaining an accurate release rate of the entrapped drugs would require both a low background of burst release drug and slow release rate from the NPs relative to the dialysis kinetics.

We therefore propose that the similarity in the apparent extent of release observed in the traditional dialysis method (Figure 4b) when comparing 20 °C to the higher temperatures is attributable to the overwhelming contribution of burst release drugs that obscure the quantification of the entrapped drug. Additionally, the inconsistency in the release rates at 28 °C and 37 °C

between the AF4 and dialysis methods suggests that the diffusion barrier of enrofloxacin across the dialysis membrane becomes the limiting rate relative to the NP release rate at high temperatures. Hence, release rates from the NPs would be underestimated if the dialysis lag time were not considered in the analysis of the dialysis data, as noted in a prior study comparing rapid probe measurements of the release of a procaine drug to dialysis measurements [15].

The first hypothesis regarding the release extent would suggest that the difference in the enrofloxacin concentrations at 37 °C and 20 °C in the dialysate after equilibration (e.g., 26 hours) should represent the actual drug entrapment inside the NPs, assuming complete release at 37 °C and minimal release at 20 °C as indicated by the AF4 measurements. Direct subtraction of the results in Figure 4b yields an entrapped drug concentration of (1.7 ± 2.4) μg/mg (n = 2 replicates). The high relative standard deviation is attributable to the low entrapment, together with the propagation of uncertainty in the two concentrations being subtracted. To minimize these errors, an additional dialysis experiment was designed in two stages: first, the NPs were dialyzed at 20 °C for 26 hours to measure the burst release (assuming negligible release from the NPs); then, the dialysis device was transferred to a reservoir with clean PBS media at 37 °C to measure the subsequent release of the entrapped drug without interference of the burst release. Following this method, the burst release was determined to be (16.9 ± 0.1) μg/mg (n = 2 replicates) and drug entrapment was (2.2 ± 0.2) μg/mg (i.e., entrapment efficiency of (11.2 ± 0.9) %) (n = 2 replicates), consistent with that determined by ultrafiltration and ultracentrifugation above.

The second hypothesis regarding the dialysis lag time was evaluated by performing control experiments on the dialysis of pure enrofloxacin solutions at 300 mg/L (i.e., the concentration introduced with 15 g/L of PLGA-Enro NPs) at the three temperatures. The release profiles of the dissolved enrofloxacin are similar to those for the PLGA-Enro NPs, supporting that the traditional

dialysis measurement is primarily capturing the kinetics for transfer of the burst release across the dialysis membrane while obscuring the true release rate of entrapped drug from the NPs.

AF4-FLD resolves both problems by (1) providing rapid separation of the NPs from the dissolved background and (2) enabling direct, real-time characterization of the enrofloxacin entrapped in the NPs, thereby eliminating the interference of dissolved drugs in the measurement as well as the dialysis lag time. Hence, both the extent and rate of release of entrapped drugs are selectively probed without requiring the complicated considerations and tedious experiments to correctly interpret the traditional dialysis results.

3.4. Theoretical diffusion models successfully integrate AF4 and dialysis measurements

We hypothesized that AF4 and dialysis provide complementary measurements of the drug distribution and that a diffusion model should be capable to integrate and reconcile the two measurements. AF4 directly and selectively probes the drug entrapped inside the NPs ($C_{entrapped}$ in Figure 5) whereas the dialysis approach provides the concentration of dissolved enrofloxacin outside the dialysis device ($C_{d,outer}$). A diffusion model can then be written to explicitly account for $C_{entrapped}$ and $C_{d,outer}$, as well as the dissolved enrofloxacin inside the dialysis bag ($C_{d,inner}$) which is measured in neither experiment (because of the *in situ* washing in AF4) but can be calculated by mass balance given both the AF4 and dialysis results. Both the diffusion rates from the polymeric NPs (k_p) and across the dialysis membrane (k_d) are considered (Figure 5).

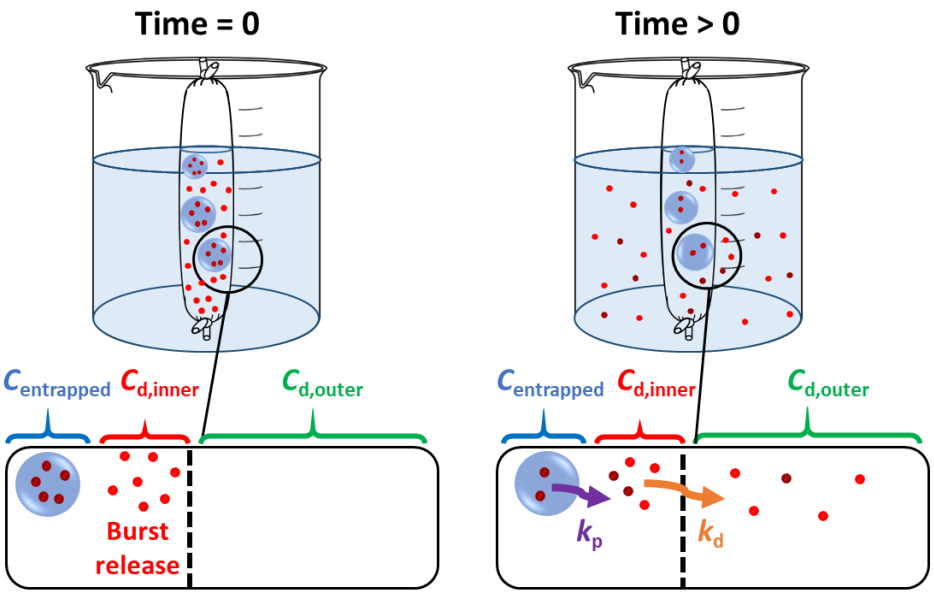

Figure 5. Schematic of dialysis, with emphasis on the distinction between the burst release and subsequent release of entrapped drug, as well as explicit consideration of the finite rates for release from the polymeric nanoparticle (k_p) and diffusion through the dialysis membrane (k_d), and three distinct drug populations of entrapped drugs within the NPs ($C_{entrapped}$), dissolved drugs inside the dialysis device ($C_{d,inner}$), and dissolved drugs outside the dialysis device ($C_{d,outer}$).

The proposed model to predict $C_{entrapped}$, $C_{d,inner}$, and $C_{d,outer}$ (Equations 1 to 3) is derived from Fick's first law and assumes homogeneous drug concentrations within the polymeric matrix of the NPs, inside the dialysis device, and in the reservoir. This model has previously been presented and applied for drug diffusion from liposomal carriers and across a dialysis membrane [61-63]. Here, a modification is made to account for accumulation of drug in the outer dialysis reservoir (i.e., perfect sink conditions are not assumed).

$$\frac{d(xC_{\text{entrapped}})}{dt} = -k_{\text{p}}(xC_{\text{entrapped}} - C_{\text{d,inner}}) \qquad (1)$$

$$\frac{dC_{\mathrm{d,inner}}}{dt} = \frac{k_{\mathrm{p}}}{x}\left(xC_{\mathrm{entrapped}} - C_{\mathrm{d,inner}}\right) - k_{\mathrm{d}}(C_{\mathrm{d,inner}} - C_{\mathrm{d,outer}}) \quad (2)$$

$$\frac{dC_{\mathrm{d,outer}}}{dt} = \frac{k_{\mathrm{d}}}{y}(C_{\mathrm{d,inner}} - C_{\mathrm{d,outer}}) \quad (3)$$

Note $C_{\mathrm{entrapped}}$ is defined here as the mass of enrofloxacin entrapped in the NPs divided by the total solution volume in the dialysis device (V_{inner} = 1 mL), while the driving force for diffusion in Fick's law requires the local concentration in the NPs (i.e., mass of enrofloxacin divided by volume of PLGA NPs, $V_{\mathrm{NPs}} = m_{\mathrm{NPs}}/\rho_{\mathrm{NPs}}$, where m_{NPs} and ρ_{NPs} are the mass and density, respectively of PLGA). Therefore, $C_{\mathrm{entrapped}}$ is adjusted by a factor x representing $V_{\mathrm{inner}}/V_{\mathrm{NPs}}$ (SI, Equation S2). The mass flux of entrapped drug to the inner dialysis solution is also divided by x in the model to obtain $C_{\mathrm{d,inner}}$. Similarly, y is the ratio of the solution volume in the reservoir (V_{outer} =120 mL) to V_{inner} and is used to obtain $C_{\mathrm{d,outer}}$ from the mass flux of drug leaving the inner dialysis solution.

Experimental values for C_{outer} were obtained directly by HPLC analysis on the dialysate in Figure 4b, and $C_{\mathrm{entrapped}}$ from the AF4 analysis in Figure 4a (assuming an initial entrapped concentration of 2.2 μg/mg from Section 3.3). The experimental $C_{\mathrm{d,inner}}$ value was computed by mass balance (SI, Equation S3). To minimize the number of fitting parameters and reduce the risk of overfitting the model, k_{d} for each temperature was obtained by fitting the data from the control experiments for enrofloxacin diffusion from the dialysis device without NPs (SI, Figure S10), and the k_{d} values were provided as fixed inputs for the NP release modeling. At each temperature, the best-fit value of k_{p} was then obtained by minimizing the sum of squared errors between the predicted $C_{\mathrm{entrapped}}$, $C_{\mathrm{d,inner}}$, and $C_{\mathrm{d,outer}}$ (Equations 1 to 3) and the experimental values across all time points measured. The best-fit models and rate constants are presented in Figures 6 and 7 and SI Table S3.

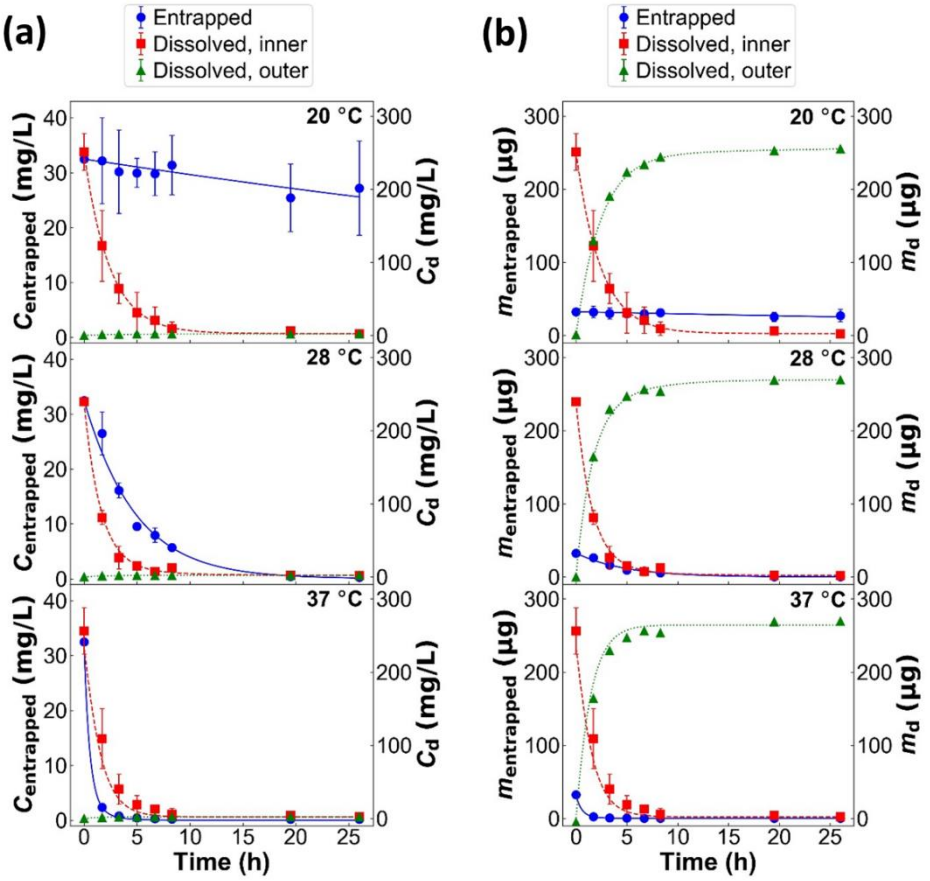

Figure 6. Experimental results (points) and model fits (lines) for the distribution of enrofloxacin between three populations (denoted in Figure 5), reported on a concentration (a) or mass (b) basis. Experimental values for $C_{entrapped}$ and $C_{d,outer}$ were obtained by AF4 and HPLC measurements, respectively, and $C_{d,inner}$ by mass balance (SI, Equation S3). Error bars represent the standard deviation across two replicates. Models were parameterized with a fixed k_d (from enrofloxacin dialysis experiments without NPs), and k_p was obtained by minimizing the sum of squared errors.

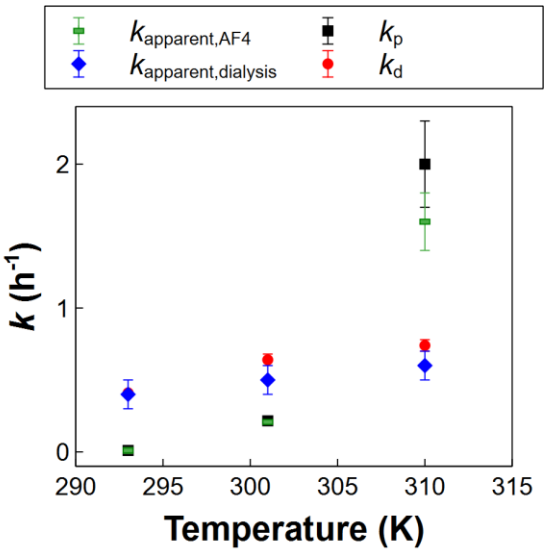

Figure 7. Rate constants for drug diffusion from PLGA NPs and dialysis membrane in the diffusion model (Figure 6), and apparent rate constants considering AF4 alone and dialysis alone. The apparent rate constants are acquired by assuming one single release process and fitting the AF4 and dialysis data individually. AF4 more accurately captures the true release rate of the entrapped drug from the NPs (k_p) and the sharp increase in k_p upon surpassing the glass transition temperature (≈ 303 K), whereas dialysis is heavily skewed toward k_d for the NPs evaluated here.

The successful fit of the model to the experimental data supports the proposed conceptual model for the release behavior and differences in AF4 and traditional dialysis measurements. The importance of the diffusion barrier imparted by dialysis is most notable at 37 °C, where k_d is slower than k_p ((0.74 ± 0.04) h^{-1} versus (2.0 ± 0.3) h^{-1}, respectively) and hence the limiting rate for drug appearance in the dialysate. At 20 °C, k_p for diffusion of entrapped drugs from the polymeric matrix is much lower than k_d of dissolved drug across the dialysis membrane ((0.01 ± 0.02) h^{-1} versus (0.41 ± 0.01) h^{-1}, respectively), and at 28 °C, k_p was also lower than k_d ((0.216 ± 0.003) h^{-1} versus (0.64 ± 0.04) h^{-1}, respectively). However, at all temperatures, the results for $C_{d,outer}$ are

primarily influenced by the large burst release (i.e., $C_{d,inner}$ at time zero) rather than the release of $C_{entrapped}$, as is clearly shown when visualizing data on a mass basis (Figure 6b).

The trend in rate constants with temperature also supports the proposed physical mechanisms for drug release from the NPs. According to the Stokes-Einstein law, the diffusion coefficient and hence diffusion rate of drug should be linearly related to temperature, assuming no change in other factors such as viscosity. Indeed, k_d across the dialysis membrane shows a linear relationship with temperature. On the other hand, k_p for release from the NPs shows a sharp increase above T_g, indicating that the rapid release is not attributable purely to increasing thermal energy but also the change in the physical properties of the polymeric matrix above T_g.

Finally, to further affirm the capabilities of AF4 over dialysis to acquire accurate k_p values, apparent rate constants are presented that would be obtained if the AF4 or dialysate measurements were analyzed individually, assuming only release from the NPs and no prior knowledge of the burst release or dialysis lag time issues (Figure 7). Release rates obtained directly from AF4 ($k_{apparent,AF4}$) using this simplified analysis more accurately represent the true k_p values from the full model, whereas those obtained from a simple fitting of the traditional dialysis data ($k_{apparent,dialysis}$) represent the diffusion rate k_d across the dialysis membrane, rather than k_p for the NPs. Considering that NPs in real applications will not be applied in a dialysis device (i.e., k_d is irrelevant) and that the entrapped drug concentration can be more important in targeted delivery than the burst release (which may occur far from the ultimate delivery site), the direct measurement of the entrapped drug release by AF4 is purported to be more useful than that obtained by dialysis.

4. Conclusions

This research demonstrates AF4-FLD as a novel approach that successfully overcomes

limitations of traditional dialysis methods (notability, lag time and susceptibility to interferences from the burst release background) to obtain release profiles of enrofloxacin from PLGA NPs, while also enabling fully size-resolved release profiles to be obtained with minimal sample preparation. A complete AF4-FLD method development was provided that explicitly addreses the optimization of the focus step to balance drug recovery and separation efficiency. The AF4-FLD approach showed highly promising results over traditional dialysis methods to reliably distinguish the extent and rate of the entrapped drug release at different temperatures, particularly under circumstances with a high background of burst release drug and when the release rate of the drug from the polymeric matrix is slower than that from the dialysis device. A theoretical diffusion model was able to explain the different results obtained by the two approaches and further demonstrated the better suitability of AF4 to accurately evaluate the release of entrapped drugs. Additional advantages of AF4 demonstrated here include the capability to add online DLS and MALS detection to simultaneously monitor the stability of the NPs during the drug release, and the ability to distinguish release rates from different NP size populations at extraordinarily high size resolution.

The AF4-FLD method developed here can be broadly applicable to characterize the release of fluorescent or fluorescently-tagged drugs from polymeric NPs and other "soft" NPs such as liposomes and micelles. The method is expected to be facile and robust to characterize drug release and NP stability across a variety of conditions (e.g., different temperatures). In future studies, the unique capabilities of AF4 to separate NPs from other constituents (e.g., biomolecules) will also be explored to acquire release profiles and drug distributions in complex matrices. These measurements can lead to better design of drug-loaded NPs and yield high value in reducing time and costs to characterize nanodelivery systems before initiating *in vivo* experiments.

Corresponding Author

* Postal Address: Department of Civil & Environmental Engineering, University of Houston, 4726 Calhoun Rd. Rm N107, Houston, TX 77004, United States; Phone: 713-743-8646; Fax: 713-743-4260; Email: slouie@uh.edu

Declaration of Competing Interest

The authors declare no competing interests.

Acknowledgements

We gratefully acknowledge Dr. Charisma Lattao for HPLC method development for dissolved enrofloxacin quantification and Dr. Xinli Liu for access to the ultracentrifuge. This material is based upon work supported by the U.S. Department of Agriculture under Grant No. 2018-67022-27969 (PSGT#17545).

Appendix A. Supporting Information

Supplementary data to this article can be found online.

References

[1] A. George, P.A. Shah, P.S. Shrivastav, Natural biodegradable polymers based nano-formulations for drug delivery: A review, Int. J. Pharm. 561 (2019) 244-264. https://doi.org/10.1016/j.ijpharm.2019.03.011.

[2] V. Pillay, A. Seedat, Y.E. Choonara, L.C. du Toit, P. Kumar, V.M.K. Ndesendo, A review of polymeric refabrication techniques to modify polymer properties for biomedical and drug delivery applications, AAPS PharmSciTech. 14 (2013) 692-711. https://doi.org/10.1208/s12249-013-9955-z.

[3] A. Godwin, K. Bolina, M. Clochard, E. Dinand, S. Rankin, S. Simic, S. Brocchini, New strategies for polymer development in pharmaceutical science—a short review, J. Pharm. Pharmacol. 53 (2001) 1175-1184. https://doi.org/10.1211/0022357011776612.

[4] S. Shakiba, C.E. Astete, S. Paudel, C.M. Sabliov, D.F. Rodrigues, S.M. Louie, Emerging investigator series: Polymeric nanocarriers for agricultural applications: Synthesis, characterization, and environmental and biological interactions, Environ. Sci. Nano. 7 (2020) 37-67. https://doi.org/10.1039/C9EN01127G

[5] Y. Xu, C.-S. Kim, D.M. Saylor, D. Koo, Polymer degradation and drug delivery in PLGA-based drug–polymer applications: A review of experiments and theories, J. Biomed. Mater. Res. Part B. 105 (2017) 1692-1716. https://doi.org/10.1002/jbm.b.33648.

[6] H.K. Makadia, S.J. Siegel, Poly lactic-*co*-glycolic acid (PLGA) as biodegradable controlled drug delivery carrier, Polymers. 3 (2011) 1377-1397. https://doi.org/10.3390/polym3031377

[7] N.D. Stebbins, M.A. Ouimet, K.E. Uhrich, Antibiotic-containing polymers for localized, sustained drug delivery, Adv. Drug Delivery Rev. 78 (2014) 77-87. https://doi.org/10.1016/j.addr.2014.04.006.

[8] P. Gao, X. Nie, M. Zou, Y. Shi, G. Cheng, Recent advances in materials for extended-release antibiotic delivery system, J. Antibiot. 64 (2011) 625-634. https://doi.org/10.1038/ja.2011.58.

[9] S. Paudel, C. Cerbu, C.E. Astete, S.M. Louie, C. Sabliov, D.F. Rodrigues, Enrofloxacin-impregnated PLGA nanocarriers for efficient therapeutics and diminished generation of reactive oxygen species, ACS Appl. Nano Mater. 2 (2019) 5035-5043. https://doi.org/10.1021/acsanm.9b00970.

[10] US Food and Drug Administration, Drug products, including biological products, that contain nanomaterials-guidance for industry, 2017. https://www.fda.gov/downloads/Drugs/GuidanceComplianceRegulatoryInformation/Guidances/UCM588857.pdf.

[11] W.B. Liechty, D.R. Kryscio, B.V. Slaughter, N.A. Peppas, Polymers for drug delivery systems, Annu. Rev. Chem. Biomol. Eng. 1 (2010) 149-173. https://doi.org/10.1146/annurev-chembioeng-073009-100847

[12] N. Kamaly, B. Yameen, J. Wu, O.C. Farokhzad, Degradable controlled-release polymers and polymeric nanoparticles: Mechanisms of controlling drug release, Chem. Rev. 116 (2016) 2602-2663. https://doi.org/10.1021/acs.chemrev.5b00346.

[13] M. Shameem, H. Lee, P.P. DeLuca, A short-term (accelerated release) approach to evaluate peptide release from PLGA depot formulations, AAPS PharmSciTech. 1 (1999) 1. https://doi.org/10.1208/ps010307.

[14] S. Lappe, D. Mulac, K. Langer, Polymeric nanoparticles–Influence of the glass transition temperature on drug release, Int. J. Pharm. 517 (2017) 338-347. https://doi.org/10.1016/j.ijpharm.2016.12.025.

[15] G. Moreno-Bautista, K.C. Tam, Evaluation of dialysis membrane process for quantifying the *in vitro* drug-release from colloidal drug carriers, Colloids Surf., A. 389 (2011) 299-303. https://doi.org/10.1016/j.colsurfa.2011.07.032.

[16] J. Gigault, J.M. Pettibone, C. Schmitt, V.A. Hackley, Rational strategy for characterization of nanoscale particles by asymmetric-flow field flow fractionation: A tutorial, Anal. Chim. Acta. 809 (2014) 9-24. https://doi.org/10.1016/j.aca.2013.11.021.

[17] S. Podzimek, Light scattering, size exclusion chromatography and asymmetric flow field flow fractionation: Powerful tools for the characterization of polymers, proteins and nanoparticles, John Wiley & Sons Inc., Hoboken, New Jersey, 2011. https://doi.org/10.1002/9780470877975.

[18] M. Wagner, S. Holzschuh, A. Traeger, A. Fahr, U.S. Schubert, Asymmetric flow field-flow fractionation in the field of nanomedicine, Anal. Chem. 86 (2014) 5201-5210. https://doi.org/10.1021/ac501664t.

[19] M.E. Schimpf, K. Caldwell, J.C. Giddings, Field-flow fractionation handbook, Wiley-Interscience, New York, 2000.

[20] K.G. Wahlund, H.S. Winegarner, K.D. Caldwell, J.C. Giddings, Improved flow field-flow fractionation system applied to water-soluble polymers: Programming, outlet stream splitting, and flow optimization, Anal. Chem. 58 (1986) 573-578. https://doi.org/10.1021/ac00294a018.

[21] M.I. Malik, H. Pasch, Field-flow fractionation: New and exciting perspectives in polymer analysis, Prog. Polym. Sci. 63 (2016) 42-85. https://doi.org/10.1016/j.progpolymsci.2016.03.004.

[22] W. Fraunhofer, G. Winter, The use of asymmetrical flow field-flow fractionation in pharmaceutics and biopharmaceutics, Eur. J. Pharm. Biopharm. 58 (2004) 369-383. https://doi.org/10.1016/j.ejpb.2004.03.034.

[23] A. Zattoni, B. Roda, F. Borghi, V. Marassi, P. Reschiglian, Flow field-flow fractionation for the analysis of nanoparticles used in drug delivery, J. Pharm. Biomed. Anal. 87 (2014) 53-61. https://doi.org/10.1016/j.jpba.2013.08.018.

[24] J. Ehrhart, A.-F. Mingotaud, F. Violleau, Asymmetrical flow field-flow fractionation with multi-angle light scattering and quasi elastic light scattering for characterization of poly (ethyleneglycol-b-ε-caprolactone) block copolymer self-assemblies used as drug carriers for photodynamic therapy, J. Chromatogr. A. 1218 (2011) 4249-4256. https://doi.org/10.1016/j.chroma.2011.01.048.

[25] C. Bayart, E. Jean, M. Paillagot, A. Renoud, A. Raillard, J. Paladino, M. Le Borgne, Comparison of SEC and AF4 analytical tools for size estimation of typhoid Vi polysaccharides, Anal. Methods. 11 (2019) 4851-4858. https://doi.org/10.1039/C9AY00145J

[26] F. Caputo, J. Clogston, L. Calzolai, M. Rösslein, A. Prina-Mello, Measuring particle size distribution of nanoparticle enabled medicinal products, the joint view of EUNCL and NCI-NCL. A step by step approach combining orthogonal measurements with increasing complexity, J. Controlled Release. 299 (2019) 31-43. https://doi.org/10.1016/j.jconrel.2019.02.030.

[27] J. Parot, F. Caputo, D. Mehn, V.A. Hackley, L. Calzolai, Physical characterization of liposomal drug formulations using multi-detector asymmetrical-flow field flow fractionation, J. Controlled Release. 320 (2020) 495-510. https://doi.org/10.1016/j.jconrel.2020.01.049.

[28] M.E. Collins, E. Soto-Cantu, R. Cueto, P.S. Russo, Separation and characterization of poly(tetrafluoroethylene) latex particles by asymmetric flow field flow fractionation with light-scattering detection, Langmuir. 30 (2014) 3373-3380. https://doi.org/10.1021/la404902x.

[29] X. Guan, R. Cueto, P. Russo, Y. Qi, Q. Wu, Asymmetric flow field-flow fractionation with multiangle light scattering detection for characterization of cellulose nanocrystals, Biomacromolecules. 13 (2012) 2671-2679. https://doi.org/10.1021/bm300595a.

[30] A. Zattoni, D.C. Rambaldi, P. Reschiglian, M. Melucci, S. Krol, A.M.C. Garcia, A. Sanz-Medel, D. Roessner, C. Johann, Asymmetrical flow field-flow fractionation with multi-angle light scattering detection for the analysis of structured nanoparticles, J. Chromatogr. A. 1216 (2009) 9106-9112. https://doi.org/10.1016/j.chroma.2009.06.037.

[31] A. Barber, S. Kly, M. Moffitt, L. Rand, J.F. Ranville, Coupling single particle ICP-MS with field-flow fractionation for characterizing metal nanoparticles contained in nanoplastic colloids, Environ. Sci. Nano. 7 (2020) 514-524. https://doi.org/10.1039/C9EN00637K

[32] M. Bouby, H. Geckeis, F.W. Geyer, Application of asymmetric flow field-flow fractionation (AsFlFFF) coupled to inductively coupled plasma mass spectrometry (ICPMS) to the quantitative characterization of natural colloids and synthetic nanoparticles, Anal. Bioanal. Chem. 392 (2008) 1447-1457. https://doi.org/10.1007/s00216-008-2422-0.

[33] S. Dubascoux, I. Le Hécho, M. Hassellöv, F. Von Der Kammer, M. Potin Gautier, G. Lespes, Field-flow fractionation and inductively coupled plasma mass spectrometer coupling: History, development and applications, J. Anal. At. Spectrom. 25 (2010) 613-623. http://doi.org/10.1039/B927500B.

[34] P. M-M, A. Siripinyanond, Field-flow fractionation with inductively coupled plasma mass spectrometry: Past, present, and future, J. Anal. At. Spectrom. 29 (2014) 1739-1752. http://doi.org/10.1039/C4JA00207E.

[35] H.E. Hadri, S.M. Louie, V.A. Hackley, Assessing the interactions of metal nanoparticles in soil and sediment matrices - a quantitative analytical multi-technique approach, Environ. Sci. Nano. 5 (2018) 203-214. http://doi.org/10.1039/C7EN00868F.

[36] Y. Hu, R.M. Crist, J.D. Clogston, The utility of asymmetric flow field-flow fractionation for preclinical characterization of nanomedicines, Anal. Bioanal. Chem. 412 (2020) 425-438. https://doi.org/10.1007/s00216-019-02252-9.

[37] A. Hinna, F. Steiniger, S. Hupfeld, M. Brandl, J. Kuntsche, Asymmetrical flow field-flow fractionation with on-line detection for drug transfer studies: A feasibility study, Anal. Bioanal. Chem. 406 (2014) 7827-7839. https://doi.org/10.1007/s00216-014-7643-9.

[38] W. Fraunhofer, G. Winter, C. Coester, Asymmetrical flow field-flow fractionation and multiangle light scattering for analysis of gelatin nanoparticle drug carrier systems, Anal. Chem. 76 (2004) 1909-1920. https://doi.org/10.1021/ac0353031.

[39] A.H. Hinna, S. Hupfeld, J. Kuntsche, M. Brandl, The use of asymmetrical flow field-flow fractionation with on-line detection in the study of drug retention within liposomal nanocarriers and drug transfer kinetics, J. Pharm. Biomed. Anal. 124 (2016) 157-163. https://doi.org/10.1016/j.jpba.2016.02.037.

[40] A.H. Hinna, S. Hupfeld, J. Kuntsche, A. Bauer-Brandl, M. Brandl, Mechanism and kinetics of the loss of poorly soluble drugs from liposomal carriers studied by a novel flow field-flow

fractionation-based drug release−/transfer-assay, J. Controlled Release. 232 (2016) 228-237. https://doi.org/10.1016/j.jconrel.2016.04.031.

[41] S. Hupfeld, D. Ausbacher, M. Brandl, Asymmetric flow field-flow fractionation of liposomes: 2. Concentration detection and adsorptive loss phenomena, J. Sep. Sci. 32 (2009) 3555-3561. https://doi.org/10.1002/jssc.200900292.

[42] A. Hawe, W. Friess, M. Sutter, W. Jiskoot, Online fluorescent dye detection method for the characterization of immunoglobulin G aggregation by size exclusion chromatography and asymmetrical flow field flow fractionation, Anal. Biochem. 378 (2008) 115-122. https://doi.org/10.1016/j.ab.2008.03.050.

[43] J. Alftrén, J.M. Peñarrieta, B. Bergenståhl, L. Nilsson, Comparison of molecular and emulsifying properties of gum arabic and mesquite gum using asymmetrical flow field-flow fractionation, Food Hydrocolloids. 26 (2012) 54-62. https://doi.org/10.1016/j.foodhyd.2011.04.008.

[44] M. Ulmius, S. Adapa, G. Önning, L. Nilsson, Gastrointestinal conditions influence the solution behaviour of cereal β-glucans *in vitro*, Food Chem. 130 (2012) 536-540. https://doi.org/10.1016/j.foodchem.2011.07.066.

[45] J.R. Runyon, M. Ulmius, L. Nilsson, A perspective on the characterization of colloids and macromolecules using asymmetrical flow field-flow fractionation, Colloids Surf., A. 442 (2014) 25-33. https://doi.org/10.1016/j.colsurfa.2013.04.010.

[46] C. Guéguen, C.W. Cuss, Characterization of aquatic dissolved organic matter by asymmetrical flow field-flow fractionation coupled to UV–Visible diode array and excitation emission matrix fluorescence, J. Chromatogr. A. 1218 (2011) 4188-4198. https://doi.org/10.1016/j.chroma.2010.12.038.

[47] Z. Zhou, L. Guo, A critical evaluation of an asymmetrical flow field-flow fractionation system for colloidal size characterization of natural organic matter, J. Chromatogr. A. 1399 (2015) 53-64. https://doi.org/10.1016/j.chroma.2015.04.035.

[48] M. Baalousha, B. Stolpe, J.R. Lead, Flow field-flow fractionation for the analysis and characterization of natural colloids and manufactured nanoparticles in environmental systems: A critical review, J. Chromatogr. A. 1218 (2011) 4078-4103. https://doi.org/10.1016/j.chroma.2011.04.063.

[49] S.T. Lee, B. Yang, J.-Y. Kim, J.-H. Park, M.H. Moon, Combining asymmetrical flow field-flow fractionation with on- and off-line fluorescence detection to examine biodegradation of riverine dissolved and particulate organic matter, J. Chromatogr. A. 1409 (2015) 218-225. https://doi.org/10.1016/j.chroma.2015.07.074.

[50] R.N. Qureshi, W.T. Kok, Application of flow field-flow fractionation for the characterization of macromolecules of biological interest: A review, Anal. Bioanal. Chem. 399 (2011) 1401-1411. https://doi.org/10.1007/s00216-010-4278-3.

[51] G. Yohannes, M. Jussila, K. Hartonen, M.L. Riekkola, Asymmetrical flow field-flow fractionation technique for separation and characterization of biopolymers and bioparticles, J. Chromatogr. A. 1218 (2011) 4104-4116. https://doi.org/10.1016/j.chroma.2010.12.110.

[52] P. Iavicoli, P. Urbán, A. Bella, M.G. Ryadnov, F. Rossi, L. Calzolai, Application of asymmetric flow field-flow fractionation hyphenations for liposome–antimicrobial peptide

interaction, J. Chromatogr. A. 1422 (2015) 260-269. https://doi.org/10.1016/j.chroma.2015.10.029.

[53] F. Danhier, E. Ansorena, J.M. Silva, R. Coco, A. Le Breton, V. Préat, PLGA-based nanoparticles: An overview of biomedical applications, J. Controlled Release. 161 (2012) 505-522. https://doi.org/10.1016/j.jconrel.2012.01.043.

[54] C.E. Astete, C.M. Sabliov, Synthesis and characterization of PLGA nanoparticles, Journal of Biomaterials Science, Polymer Edition. 17 (2006) 247-289. https://doi.org/10.1163/156856206775997322.

[55] S. D'Souza, A review of *in vitro* drug release test methods for nano-sized dosage forms, Adv. Pharmaceutics. 2014 (2014). https://doi.org/10.1155/2014/304757.

[56] M. Ramos, A. Aranda, E. Garcia, T. Reuvers, H. Hooghuis, Simple and sensitive determination of five quinolones in food by liquid chromatography with fluorescence detection, J. Chromatogr. B. 789 (2003) 373-381. https://doi.org/10.1016/S1570-0232(03)00212-5.

[57] J. Kuntsche, C. Decker, A. Fahr, Analysis of liposomes using asymmetrical flow field-flow fractionation: Separation conditions and drug/lipid recovery, J. Sep. Sci. 35 (2012) 1993-2001. https://doi.org/10.1002/jssc.201200143.

[58] S. Holzschuh, K. Kaeß, A. Fahr, C. Decker, Quantitative *in vitro* assessment of liposome stability and drug transfer employing asymmetrical flow field-flow fractionation (AF4), Pharm. Res. 33 (2016) 842-855. https://doi.org/10.1007/s11095-015-1831-y.

[59] W. Burchard, M. Schmidt, W. Stockmayer, Information on polydispersity and branching from combined quasi-elastic and integrated scattering, Macromolecules. 13 (1980) 1265-1272. https://doi.org/10.1021/ma60077a045.

[60] B. Roda, V. Marassi, A. Zattoni, F. Borghi, R. Anand, V. Agostoni, R. Gref, P. Reschiglian, S. Monti, Flow field-flow fractionation and multi-angle light scattering as a powerful tool for the characterization and stability evaluation of drug-loaded metal–organic framework nanoparticles, Anal. Bioanal. Chem. 410 (2018) 5245-5253. https://doi.org/10.1007/s00216-018-1176-6.

[61] V. Joguparthi, B.D. Anderson, Liposomal delivery of hydrophobic weak acids: Enhancement of drug retention using a high intraliposomal pH, J. Pharm. Sci. 97 (2008) 433-454. https://doi.org/10.1002/jps.21135.

[62] S. Modi, T.-X. Xiang, B.D. Anderson, Enhanced active liposomal loading of a poorly soluble ionizable drug using supersaturated drug solutions, J. Controlled Release. 162 (2012) 330-339. https://doi.org/10.1016/j.jconrel.2012.07.001.

[63] S. Modi, B.D. Anderson, Determination of drug release kinetics from nanoparticles: Overcoming pitfalls of the dynamic dialysis method, Mol. Pharmaceutics. 10 (2013) 3076-3089. https://doi.org/10.1021/mp400154a.